



HAL
open science

Targeting tumors with cyclic RGD-conjugated lipid nanoparticles loaded with an IR780 NIR

Jungyoon Choi, Emilie Rustique, Maxime Henry, Mélanie Guidetti, Véronique Josserand, Lucie Sancey, Jérôme Boutet, Jean-Luc Coll

► **To cite this version:**

Jungyoon Choi, Emilie Rustique, Maxime Henry, Mélanie Guidetti, Véronique Josserand, et al.. Targeting tumors with cyclic RGD-conjugated lipid nanoparticles loaded with an IR780 NIR. *International Journal of Pharmaceutics*, 2017, [Epub ahead of print]. 10.1016/j.ijpharm.2017.03.007 . inserm-01488572

HAL Id: inserm-01488572

<https://inserm.hal.science/inserm-01488572>

Submitted on 13 Mar 2017

HAL is a multi-disciplinary open access archive for the deposit and dissemination of scientific research documents, whether they are published or not. The documents may come from teaching and research institutions in France or abroad, or from public or private research centers.

L'archive ouverte pluridisciplinaire **HAL**, est destinée au dépôt et à la diffusion de documents scientifiques de niveau recherche, publiés ou non, émanant des établissements d'enseignement et de recherche français ou étrangers, des laboratoires publics ou privés.



Targeting tumors with cyclic RGD-conjugated lipid nanoparticles loaded with an IR780 NIR

Jungyoon Choi, Emilie Rustique, Maxime Henry, Mélanie Guidetti, Véronique Josserand, Lucie Sancey, Jérôme Boutet, Jean-Luc Coll

► To cite this version:

Jungyoon Choi, Emilie Rustique, Maxime Henry, Mélanie Guidetti, Véronique Josserand, et al.. Targeting tumors with cyclic RGD-conjugated lipid nanoparticles loaded with an IR780 NIR. International Journal of Pharmaceutics, Elsevier, 2017, <10.1016/j.ijpharm.2017.03.007>. <inserm-01488572>

HAL Id: inserm-01488572

<http://www.hal.inserm.fr/inserm-01488572>

Submitted on 13 Mar 2017

HAL is a multi-disciplinary open access archive for the deposit and dissemination of scientific research documents, whether they are published or not. The documents may come from teaching and research institutions in France or abroad, or from public or private research centers.

L'archive ouverte pluridisciplinaire **HAL**, est destinée au dépôt et à la diffusion de documents scientifiques de niveau recherche, publiés ou non, émanant des établissements d'enseignement et de recherche français ou étrangers, des laboratoires publics ou privés.

Targeting tumors with cyclic RGD-conjugated lipid nanoparticles loaded with an IR780 NIR dye: *in vitro* and *in vivo* evaluation.

JungyoonChoi(1), Emilie Rustique(2), Maxime Henry(1), Mélanie Guidetti(1),Véronique Josserand(1), Lucie Sancey(1), Jérôme Boutet(2) andJean-Luc Coll(1)

(1) Institute for Advanced Biosciences, INSERM U1209, CNRS UMR 5309, Université Grenoble Alpes, 38000 Grenoble, France

(2) CEA, LETI, MINATEC Campus, Technologies for Biology and Health Division, 17 Avenue des Martyrs, 38054 Grenoble, France

Correspondingauthor: Jean-Luc Coll :Centre de Recherche UGA-INSERM U1209, CNRS UMR 5309 ; Institute For Advanced Biosciences; Site Santé, Allée des Alpes ; 38700 La Tronche ; FRANCE

Email : Jean-luc.coll@univ-grenoble-alpes.fr

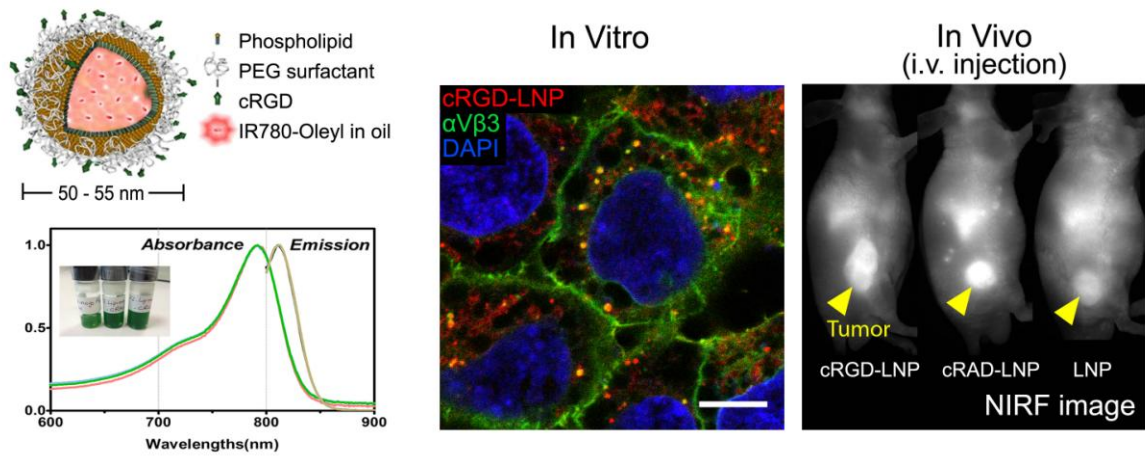
Tel : +33 6 37 77 54 58

Fax : +33 4 76 54 94 13

Abstract

Like several 50 nm-large nanocarriers, lipid nanoparticles (LNPs) can passively accumulate in tumors through the Enhanced Permeability and Retention effect. In this study, we developed PEGylated LNPs loaded with IR780 iodide as a contrast agent for NIR fluorescence imaging and modified them with cyclic RGD peptides in order to target integrin $\alpha_v\beta_3$. We demonstrate a specific targeting of the receptor with cRGD-LNPs but not with cRAD-LNP and standard LNP using HEK293(β_3), HEK293(β_3)- α_v RFP, DU145 and PC3 cell lines. We also demonstrate that cRGD-LNPs bind to $\alpha_v\beta_3$, interfere with cell adhesion to vitronectin and co-internalize with $\alpha_v\beta_3$ within one hour. We then investigated their biodistribution and tumor targeting in mice bearing DU145 or M21 tumors. We observed no significant differences between cRGD-LNP and the non-targeted ones regarding their biodistribution and accumulation/retention in tumors. This suggested that despite an efficient formulation of the cRGD-LNPs, the cRGD-mediated targeting was not increasing the total amount of LNP that can already accumulate passively in the subcutaneous tumors via the Enhanced Permeability and Retention effect (EPR).

Graphical abstract



Keywords (6 maximum)

Cancer imaging, theranostic, integrins, RGD, nanoemulsion, NIR imaging

1. Introduction

There has been a lot of effort to generate nanovectors suitable for the delivery of contrast agents and drugs. Several drug delivery systems are approved by the FDA, but only a few targeted formulations are currently tested in humans (Shi, Kantoff, Wooster, & Farokhzad, 2016). Among the different formulations, Lipid Nanoparticles (LNPs) are promising in particular because they are showing: 1) excellent biocompatibility, 2) long circulation time in blood, 3) passive tumor accumulation via the enhanced permeability and retention (EPR) effect, 4) capacity of loading large amount of poorly soluble drugs as well as imaging probes, 5) possible chemical surface modifications that may help for active specific receptor targeting (Goutayer et al., 2010; Hirsjarvi et al., 2013) (Gravier et al., 2011; Jacquart et al., 2013; Merian et al., 2015). LNPs are made of a lipophilic core encapsulated by a PEGylated mono-layer of phospholipids.

LNPs loaded with a lipophilic-derivative of IR780 dye (addition of a C18 chain to IR780 iodide dye) are stable for 6 months in phosphate buffer saline at 4°C in the dark. They present a long-lasting EPR-mediated retention in subcutaneous tumors (Jacquart et al., 2013) due to the presence of a PEG-coating. Unfortunately, PEGylation is also lowering their interaction with cell membranes and this is finally ending-up with a low efficiency of intracellular delivery of the cargo (Bozzuto & Molinari, 2015). We expect that the presence of a targeting ligand should improve this final step.

The cyclic Arg-Gly-Asp (RGD) peptide known to target preferentially the $\alpha_v\beta_3$ integrin (Dechantsreiter et al., 1999; Haubner et al., 1996) has been largely used for this purpose as recently reviewed in Arosio et al. (Arosio, 2016 #2540). RGD was used in particular for applications such as cancer imaging, radiotherapy, phototherapy and nanomedicine

(Abdollahi et al., 2005; Chen, Deng, Zhao, & Tao, 2012; Kunjachan et al., 2015; Liu & Wang, 2013; Ray et al., 2011; Shuhendler et al., 2012; Wang, Chen, Zhang, Chen, & Zhu, 2014; Yan et al., 2016; Yuan, Yang, Wu, Hu, & Ming, 2015). Our group also described cyclic-RGDfK-decorated LNPs loaded with DiD, a dye adapted to Near-infrared *in vivo* imaging (Goutayer et al., 2010). This cRGD-LNP showed a good tumor accumulation and longer retention in tumors. We then generated Indocyanine Green (ICG)-containing LNP because ICG is approved for human injection, but ICG was leaking out rapidly from the LNP *in vivo* (Gravier et al., 2011; Merian et al., 2015). We thus finally generated stable and bright LNPs containing IR780-Oleyl modified dye, which turned out to be suitable for *in vivo* imaging (Jacquart et al., 2013).

In the present study, we developed the IR780-Oleyl -LNPs targeted by cyclic RGD. We demonstrate that cRGD-LNP are functional because they bind to integrin $\alpha_v\beta_3$ and are internalized. However, despite these satisfying results *in vitro*, the presence of cRGD targeting does not augment the global accumulation of targeted versus non-targeted NP.

2. Materials and methods

2.1. Materials

Suppocire NB™ (semi-synthetics C12-C18 saturated triglyceride) was purchased from Gattefossé (Saint-Priest, France); Lipoid S75 (soybean lecithin at >75% phosphatidylcholine) from Lipoid (Ludwigshafen, Germany); Myrj™ S40 (polyethylene glycol 40 stearate); Super refined soybean oil from CrodaUniqema (Chocques, France); Cyclic RGD and cyclic RAD from Pepscan Presto (Lelystad, Netherland). IR780 iodide dye ((2-[2-[2-Chloro-3-[(1,3-dihydro-3,3-dimethyl-1-propyl-2*H*-indol-2-ylidene)ethylidene]-1-cyclohexen-1-yl]ethenyl]-3,3-dimethyl-1-propylindolium iodide) and other chemicals for the LNP preparation were purchased from Sigma-Aldrich (Saint-Quentin-Fallavier, France). Cyclic RGD stands for c[DfK(Mal)RG] and cRAD for c[DfK(Mal)RA] with f= D phenylalanine and Mal= 3 Maleimide Propionic Acid.

Cell culture media and buffers were purchased from Gibco (Life technologies, Paisley, UK); Bovine serum albumin (BSA) from Interchim (Montluçon, France); Puromycin dihydrochloride from Sigma-Aldrich (USA); Recombinant human vitronectin (rhVTN-N, truncated) and Geneticin (G418 sulfate) from Life Technologies. Unless otherwise specified, phosphate buffer saline (PBS) and Hanks' Balanced Salt Solution (HBSS) are always supplemented with 1 mM CaCl₂ and 1 mM MgCl₂.

2.2. Targeted and non-targeted LNP preparation

The formulation and composition of LNPs (previously called Lipimage815) has been already described in details (Jacquart et al., 2013). Briefly, the IR780-Oleyl dye was synthesized starting from the commercial IR780 iodide by adding a C₁₈ lipid chain. A mixture of oil, Suppocire NB™ and lecithin was prepared, then, the dye was introduced in it. An aqueous

solution with a mix of Myrj™ S40 (PEG-40 Stearate) and SA_{COHN}-PEG₁₀₀-SPDP (3% of the totality of PEG) in 154 mM NaCl buffer was added to the oil phase. Fifty nm-large lipid particles were formed through the emulsification process during a 5 min-sonication using a VCX750 Ultrasonic processor (power output 190 W, 3mm probe diameter, Sonics). A solution of DTT was added to the LNPs and agitated for 2 hours to obtain LNPs-SH. The LNP dispersions were dialyzed overnight at RT against 1000 times their volume in 154mM NaCl buffer (12 to 14 KDa MW cut off membranes, ZelluTrans, Carl Roth, France).

Following the first step of LNP-SH synthesis, the peptide conjugation was carried out by the thiol-maleimide coupling reaction. 2 mL of LNP-SH (15% lipids) solution were mixed with 75 µL of each peptide linked with maleimide (cyclic RGD and cyclic RAD – 750 nmol in DMSO). After 4 hours of a coupling reaction at RT in the dark, the remaining SH groups were neutralized using a solution of 1-(2-hydroxyethyl)-1H-pyrrole-2,5-dione for 30 min. Another dialysis was completed overnight to purify the peptide-conjugated LNPs. The final LNP dispersions were filtered through a 0.22 µm Millipore membrane for sterilization and stored at 4°C in the dark.

2.3. Characterization of LNPs

LNPs' hydrodynamic diameters, polydispersity indexes (PDI) and zeta potentials were determined in sterile 0.1X PBS (no CaCl₂/mgCl₂) using a dynamic light scattering (DLS) instrument (Zeta Sizer NanoZS, Malvern, UK), performed in triplicate. The absorbance and fluorescence spectra were measured in 1X PBS using a spectrophotometer Thermo Scientific Evolution 201 and a fluorescence spectrometer Perkin Elmer LS55, respectively. The emission spectrum was measured with excitation at 790nm. Each measurement was

performed in triplicate. Concentrations mentioned for LNPs represent the concentrations of particles.

2.4. Cell lines and culture conditions

HEK293(β_3) cells, a human embryonic kidney cell line HEK293 that was stably transfected with the human β_3 integrin gene (kindly provided by J-F. Gourvest, Aventis, France), were cultured in DMEM-GlutaMAX™ supplemented with 10% FBS and 700 $\mu\text{g}/\text{mL}$ Geneticin. HEK293(β_3)- α_v RFP cells, a variant cell line of HEK293(β_3) transfected with the human α_v integrin gene tagged by RFP at its extracellular domain (N-terminus part), were cultured as the HEK293(β_3) cells but in the presence of 1 $\mu\text{g}/\text{mL}$ Puromycin (See Supplementary information). DU145 cells, a human prostate carcinoma cell line (purchased from ATCC), and M21 cells, a human melanoma cell line, were cultured in DMEM-GlutaMAX™ with 10% FBS. PC3 cells, a human prostate adenocarcinoma cell line (ATCC), were cultured in DMEM-F12-GlutaMAX™ with 10% FBS. Cells were maintained at 37°C, 5% CO₂ in a humidified incubator.

2.5. Evaluation of $\alpha_v\beta_3$ expression by flow cytometry

Cells were grown and harvested at 60% confluency. The cells were briefly washed with 1X PBS and resuspended with trypsin. After being centrifuged at 1200 rpm for 5 min, the cells were suspended in 1X PBS. 5×10^5 cells per tube were suspended in 100 μL cold 1X PBS and mixed with 20 μL of anti- $\alpha_v\beta_3$ monoclonal antibody (PE-conjugated mouse anti-human CD51/CD61, clone 23C6, BD Pharmingen) during 1-hr on ice in the dark. After

rinsingtwicethey were finally suspended in 200 μ L cold PBS.Their fluorescence intensitywas measured using a flow cytometer (BD Accuri C6; BD Biosciences).

2.6. Cell attachment assay with vitronectin

A 96-well plate (Nunc Maxisorp ELISA plates) was coated with 5 μ g/mL vitronectin (50 μ L per well) overnight at 4°C. Then, the wells were drained and incubated with 3% (w/v) BSA (50 μ L per well) for an hour at 37°C. The negative control wellswere coated with 3% BSA only. The plate was rinsed once with HBSS. 50 μ L of 25 000 cells and 50 μ L of the LNP per well were added in the wells and incubated at 37°C for 15 min (HEK293(β_3) and DU145) or 30 min (PC3). When needed, the cells and LNPs were diluted in HBSS. The plates were drained and gently washed twice with 200 μ L of 1X HBSS per well. The surface-bound cells were fixed with ethanol for 15 min at RT and dried at RT or 37°C. The fixed cells were then stained with 1% methylene blue (50 μ L per well) for 15 min at RT, rinsed in running waterand dried. The blue dye was finally eluted in 0.1 N HCl (50 μ L per well) and the plates were scanned at a 620nm absorbance wavelength using a Beckman Coulter AD340 plate reader. All the measurements were performed in triplicate (or quadruplicate) and repeated twice.

2.7. Microscopy

2.7.1. Bright field microscopy

HEK293(β_3) cells(5×10^4 cells/well) were seeded in a8-well chambered coverglass(Nunc Lab-Tek, Thermo Fisher Scientific) and grown overnight in DMEM with 10% FBS and 700 μ g/mL Geneticin at 37°C. The cells were washed once with pre-warmed 1X PBS and the chambered coverglass was moved to a microscope (Zeiss AxioObserver Z1) equipped with a humidified culture chamber. After being placed on the microscope, the cells were treated with the LNPs

diluted to 45 or 4.5 nM in HBSS. Then, 3% (v/v) FBS were shortly added to each well. The images were taken every 5 min starting from the treatment time point (T0).

2.7.2. Confocal laser scanning microscopy

HEK29(β_3)- α_v RFP cells were seeded (at 5×10^4 cells/500 μ L/well) in a 4-well chambered coverglass (Nunc Lab-Tek, Thermo Fisher Scientific) and kept overnight in DMEM with 10% FBS, 700 μ g/mL Geneticin and 1 μ g/mL Puromycin at 37°C. The cells were washed once with pre-warmed PBS and treated with 500 μ L of different LNPs diluted at 45 or 4.5 nM in HBSS. After an incubation time of 5, 10, 30 or 60 min, the cells were gently washed once with HBSS and fixed with 4% PFA containing 1 μ g/ml of Hoechst 33342 for 15 min at RT in the dark. Then the cells were washed and stored in 1X PBS and observed using a confocal microscope LSM510 NLO META FLIM (Zeiss Axiovert 200M). A 63x oil immersion objective was used. The Hoechst-stained nuclei were excited with a 720-nm biphoton laser and detected with a 390-465 nm filter. The RFPs were excited with a 543-nm laser and signals were collected with a 565-615 nm filter.

For the internalization study, the HEK293(β_3)- α_v RFP cells were seeded in the 4-well chamber coverglass and incubated overnight. The incubation, fixation and Hoechst-staining were as described above. The cells were then observed using a confocal microscope LSM710 NLO (Zeiss AxioObserver Z1) with a 63x oil immersion objective. The LNP signal was excited using a 633-nm laser, set up at 50 % of its maximum intensity and a 636 – 758 nm detection filter was used. The Hoechst was excited with a 405-nm laser and detected with a 415 – 502 nm filter. The RFP was excited with a 560-nm laser and detected with a 563 – 631 nm filter. The scanned images were pseudo-colored in blue for nuclei, in green for α_v RFP and in red for the LNP.

2.8. Human tumor xenograft mice

All animal procedures are in compliance with the guidelines of the European Union (regulation n°86/609), taken in the French law (decree 87/848) regulating animal experimentation. All efforts are made to minimize animal suffering and to reduce the number of animals used. All animal manipulations are performed with sterile techniques and are approved by the ethical committee of Grenoble for the use of animal research (France). Subcutaneous tumor mice bearing DU145 or M21 tumor were used for an *in vivo* evaluation of the LNPs. Eight weeks old male NMRI nude mice were purchased from Janvier, Le Genest-Saint-Isle, France. Mice were anesthetized (isoflurane/oxygen 3.5%–4% for induction and 1.5%–2% thereafter, CSP, Cournon, France) and were subcutaneously injected with 10^7 of DU145 cells or 4×10^6 of M21 cells per mouse in the right trunk. When the tumors reached a volume between 200 and 500 mm³, the mice were used for LNP injections. Tumor growths took 70 days for the DU145 tumors and 43 days for the M21 tumors in average.

2.9. NIR *in vivo* imaging after injections of LNPs

Isoflurane-anesthetized mice were injected in the tail vein with 200 µl of 450 nM LNPs (equal to 10 nmol of fluorophores). NIR fluorescence images were acquired 1, 3, 5 and 24hrs after injection with a Fluobeam®800 device from Fluoptics (Grenoble, France) equipped with a 780nm excitation laser and an LP820nm detection filter. The mice were sacrificed after the last acquisition and fluorescence present in the extracted organs and serum were also acquired. Major organs were cryo-conserved for *ex vivo* studies. Image analysis was performed using the Wasabi software (Hamamatsu, Massy, France).

2.10. Statistical analysis

Statistical analysis of the data was performed by using two-way ANOVA with Bonferroni post-tests. A difference of p value < 0.05 was considered statistically significant. All the data are shown as mean \pm SD.

3. Results

3.1. Characteristics of LNPs

The outer layer composition and chemical structure of peptide-coated LNPs are illustrated in Figure 1. LNPs are made of a phospholipid monolayer that delineates their oily core containing the fluorophores, and an outer shell of PEG surfactant with or without the peptide ligand for tumor targeting. The cyclic RGDfK ($\alpha_v\beta_3$ -targeting peptide) or cyclic RADfK (a negative control of cRGD in which the glycine was replaced by an alanine, Figure 1-iv) peptides were linked on the PEGs by a maleimide-thiol coupling reaction (Figure 1-iii).

The two peptide-conjugated LNPs showed a slightly larger diameter of 55 nm as compared to the 50 nm of the standard LNP without peptide. The polydispersity indexes (PDI) of the three LNPs were lower than 0.13, indicating that they are monodispersed and do not form aggregates. The zeta potentials were kept closed to neutrality around -4 mV for each LNPs without significant difference due to the presence of the peptides (Table 1). Such zeta-potentials are avoiding non-specific electrostatic interactions.

Due to the inclusion of IR780-Oleyl, the maximum absorbance was observed for wavelengths centered at 790-792 nm and the maximum emission band was detected at 810-812 nm (Supplementary Figure 1). Based on the measured concentrations of IR780 and of LNPs, we calculated that each nanoparticle contained approximately 108 molecules of dye (Table 1).

3.2. cRGD-LNPs prevent cell binding on vitronectin

We investigated if the presence of cRGD could prevent the binding of three different cell lines on vitronectin, a “natural” protein ligand recognized by the $\alpha_v\beta_3$ integrin. As established by flow cytometry, HEK293(β_3) and DU145 express the integrin while PC3 cells does not (Figure 2A). Cells were mixed in solution with 4.5, 9.0, 45.0 and 90.0 nM of cRGD-, cRAD- or Standard-LNPs and then added on vitronectin coated multiwell plates (Figure 2B). The treatment of the cells with cRGD-LNP only decreased the adherence of HEK293(β_3) and DU145 cells. HEK293(β_3) cell adhesion was strongly decreased in the presence of 45 nM cRGD-LNP ($p < 0.001$) but was already statistically decreased with 9 nM cRGD-LNPs ($p < 0.01$). Because DU145 cells are expressing lower amounts of integrins they are more sensitive to the presence of cRGD and 4.5 nM cRGD-LNP ($p < 0.001$) were sufficient to impact strongly on their adhesion. In contrast, the adherence of $\alpha_v\beta_3$ -negative PC3 cells was not particularly affected by cRGD-LNPs (Figure 2B).

3.3. cRGD-mediated detachment of $\alpha_v\beta_3$ -positive cells

Having confirmed that cRGD-LNPs can bind onto the freely-accessible $\alpha_v\beta_3$ receptor when the cells are in suspension, we next explored their capacity to reach and interfere with occupied $\alpha_v\beta_3$ -integrins on cells grown in a monolayer. Confluent HEK293(β_3) cells were treated with 4.5 nM or 45 nM cRGD, cRAD, or standard LNP in a solution containing 3% FBS. The cells were observed for more than 3 hours on a microscope equipped with a culture chamber (Figure 3). In the presence of 45 nM cRGD-LNP the cells started retracting during the first 5 min and gradually lost adhesion over time. When used at 4.5 nM, cRGD-LNP still affected cell adhesion, although less severely, and this effect was only transient and the cell-

cell contacts were restored after 3 hours. The cRAD and standard LNPs did not affect cell shape when tested at 45 and 4.5 nM LNP (Figure 3 and Supplementary Figure 2).

We then used HEK293(β_3)- α_v RFP cells expressing integrin α_v -labeled with red fluorescent protein (RFP) (but pseudo color in green in the figures). In this cell line, the $\alpha_v\beta_3$ integrin was located mainly on the plasma membrane and enriched in area of cell-cell contacts. Cell retraction was clearly visible one hour after addition of 45 nM cRGD-LNP (Figure 4A right panel). As can be seen on the bottom panel, cell shrinkage, loss of focal and of cell-cell junctions occurred very rapidly and were visible as soon as 5 min after addition of the cRGD-LNPs (Figure 4B).

This indicated that cRGD-LNPs were functional and could bind to $\alpha_v\beta_3$ even when the integrin was already engaged.

3.4. Internalization of cRGD-LNP

Using the HEK293(β_3)- α_v RFP cells, we further investigated the internalization of cRGD-LNPs. Please note that the “red” signal of the α_v RFP protein is presented in green. In contrast with the LNPs and cRAD-LNPs which did not provide a significant cell labeling, an intense labeling of the cell membranes was observed with cRGD-LNPs at 45 nM (Figure 5). Similar results were also obtained when the different LNPs were used at 4.5 nM (Supplementary Figure 3). Importantly, intracellular vesicles (probably endosome) were also positively stained by both the cRGD-LNP and by the integrin-fusion protein after 60 min of incubation (Figure 5, first row), but not after 10 or 30 min (Supplementary Figure 4), suggesting that the internalization was mediated by the $\alpha_v\beta_3$ integrin via a slow process that necessitated between 30 and 60 min. The vesicles co-stained by cRGD-LNPs/integrin $\alpha_v\beta_3$ were also found

when the cells were washed 15 min after addition of the cRGD-LNPs (Figure 5, second row). In these conditions, the plasma membranes were not strongly labeled: the integrin/cRGD-LNP complexes initially located to the membrane were internalized, while the cell medium containing the cRGD-LNP was removed, preventing any binding after the rinsing.

3.5. *In vivo* evaluation

In order to demonstrate the cRGD-specific targeting of tumors *in vivo*, we compared the biodistribution of the three LNPs in mice bearing DU145 or M21 tumors. M21 is a human melanoma cell line that strongly expresses the $\alpha_v\beta_3$ integrin ((Felding-Habermann et al., 1992),Supplementary Figure 5).After i.v.injections of 200 μ l of 450 nM LNPs, we followed the distribution of the NIR-labeled LNPs in real time using a NIR camera. Unexpectedly, no major differences in the tumor accumulation were found between the cRGD-, cRAD- and standard LNPs in both DU145 or M21 tumors(Figure 6 and Supplementary Figure 6). This was confirmed *ex-vivo* after sacrifice of the mice and excision of the tumors(Figure 7 and Supplementary Figure 7). As well, no significant differences of EPR-mediated accumulation were detected when the mice bearing M21 tumors were followed for 4-5 days after the injections.

Thus,the 3 types LNPs accumulate passively via the EPR effect in the 2 tumor types. However, the presence of cRGD does not provide a significant augmentation of the number of LNPs that can be detected macroscopically in the tumors.

4. Discussion

The main objective of this study was to demonstrate aspecific binding and internalization of the cRGD-LNP in order to generate tumor targeted nanoparticles for theranostic purpose.

We found that cRGD-LNP can bind and interfere functionally with integrin $\alpha_v\beta_3$ *in vitro*. This indicated that the chemical coupling of cRGD on the PEGylated lipid nanocapsules was correct and resulted in an efficient recognition of the integrin receptors on the cell surface. cRGD-LNPs were able to bind to “free” integrins present on the surface of the cells in suspension as well as on those already bound to vitronectin. This later effect caused an efficient shrinking of adherent cells due to the inhibition of cell-cell and cell-matrix contacts. This effect was strong enough to detach integrin positive cells when cRGD-LNPs were used at a 45 nM concentration. At a lower concentration (4.5 nM), the detachment was transient and cell adhesion and spreading was recovered after 3 hours. As expected this effect was more pronounced on DU145 cells expressing low levels of integrins than on HEK293(β_3) cells which are strongly $\alpha_v\beta_3$ positive.

Of note, the HEK293(β_3) cell line is integrin β_5 negative while DU145 and PC3 are known to express low to moderate levels of $\alpha_v\beta_5$ and $\alpha_5\beta_1$ and negligible levels of $\alpha_{11b}\beta_3$ (Sutherland et al., 2012). All these different integrins can recognize the RGD motif, but the important specificity of cyclic RGDfK toward $\alpha_v\beta_3$ is thus largely predominant (Mas-Moruno et al., 2010).

Integrin internalization can occur via macro-pinocytosis, clathrin-dependent or clathrin-independent endocytosis (Bridgewater et al., 2012). We previously demonstrated that internalization of a tetravalent cRGD presenting scaffold, is mediated via clathrin-mediated endocytosis (Sancey et al., 2009). Other integrin-targeted NPs such as trimethyl chitosan

based NPs labeled with FQSIYPPiK (an $\alpha_v\beta_3$ targeting peptide) are using clathrin-mediated endocytosis (Xu et al., 2016). In the present study, we also observed that only the cRGD-LNPs are actively endocytosed and can be seen trafficking within α_v -RFP and IR780-Oleylco-labeled vesicles. In addition, a weaker and diffuse IR780 fluorescence signal was also building up over time in the cytoplasm and this diffuse signal was also detected in the presence of the negative controls cRAD- and non-targeted-LNPs. This may indicate that while only cRGD-LNPs can enter specifically via a cRGD-integrin dependent pathway(s), all 3 types of LNPs can fuse non-specifically with the lipids of the cell membranes and can then release their content directly to the cytoplasm. This could have an important impact for LNP-mediated drug delivery. In particular, we are currently investigating the possible cytotoxic effect generated under a 800 nm light-activation of the IR780 dye since this dye is known to generate toxic reactive oxygen species usable for photodynamic therapy.

In vivo, no specific accumulation was noticed in the integrin positive DU145 or M21 subcutaneous tumors after intravenous injection of the cRGD-LNPs versus cRAD- or Standard-LNPs. Similar fluorescence intensities as well as similar kinetics of accumulation in the tumors were measured with the 3 types of LNPs. This suggested that the functionalization of the LNPs by cRGD motifs did not generate a significantly augmented capture or retention of the targeted versus not-targeted LNPs in the tumor mass. This is in agreement with our former work in which we used cRGD-targeted DID-loaded nanoemulsions. In this previous work, we had a very modest augmentation of cRGD-dependent targeting *in vivo* when using HEK293(β_3) tumors but not TSA/pc's (Goutayer et al., 2010). Actually, HEK293(β_3) cells are very strongly expressing the integrin while TSA/pc are weakly expressing it. On the other hand, we classified HEK293(β_3) subcutaneous tumors as "EPR-deficient" because an

intravenous injection of lipid nanoemulsions generated a tumor/skin ratio of 1.5, while TSa/Pc were found EPR-positive with a Tumor/Skin ratio of 3.0 (Karageorgis et al., 2016). According to this scheme, DU145 and M21 tumors can thus be classified as EPR-positive based on their T/S ratio of ± 3 , as well as integrin positive. This suggests that active, cRGD-mediated, targeting is not augmenting the accumulation of the nanoemulsions when the EPR effect is present. However, several groups including ours (Dufort et al., 2011; Karageorgis et al., 2017) have shown that RGD-vectorization is efficiently inducing a therapeutic effect (for very recent examples, see: (Fang et al., 2017; Zhu et al., 2016), and a recent review by Zhong et al. (Zhong et al., 2014). This suggests that cRGD-active targeting may be important at the very last step, *i.e.* to deliver the cargo more efficiently into the cytoplasm of integrin positive cells. We are now actively trying to validate this hypothesis that may be important for therapeutic applications in particular when the toxic agent cannot cross the plasma membrane on its own.

5. Acknowledgements

Jungyoon Choi was supported by the Ligue Nationale contre le Cancer (GB/MA/SC-12742), the Fondation ARC pour la Recherche sur le Cancer (DOC20150602724) and by Campus France (reference: 796786A). This work was supported by a public grant overseen by the French National Research Agency (ANR) as part of the “Investissements d’Avenir” program (reference: ANR-10-NANO-01), but also by the Institut National de la Santé et de la Recherche Médicale (INSERM U1209) and by the France Live Imaging program. The authors acknowledge the team of the “OPTIMAL small animal optical imaging facility” in our institute.

6. Figure legends

Figure 1. LNP composition. (i) Schematic representation of the LNPs. (ii-iv) Chemical structure of the targeted or non-targeted surfactants used in the different LNPs. The cyclic RGDfK (iii, targeting) and cRADfK (iv, control) peptides were conjugated on the PEG by the maleimide-thiol coupling reaction. The illustration was adapted from (Merian et al., 2015).

Figure 2. Integrin specific binding of cRGD-LNPs. (A) The presence of the $\alpha_v\beta_3$ integrin was detected by flow cytometry on HEK293(β_3), DU145 and PC3 cells. Red: antibody-labeled cells; black: control cells (no antibody). (B) The capacity of cells to stick to the vitronectin coating was measured for each cell line (HEK293(β_3), DU145 and PC3) in the presence of different LNPs at 4.5, 9, 45 and 90 nM. The number of adherent cells was measured by methylene blue staining. Mean \pm SD, n=6-8. The values were normalized with those of the standard LNP. Asterisks: ** = $p < 0.01$, *** = $p < 0.001$, compared to the std LNP.

Figure 3. Confluent HEK293(β_3) cells treated with LNPs at 45 or 4.5 nM. The cells were observed for a period of 3 hours in real time under the microscope equipped with a culture system for live cell imaging. Scale bar = 100 μ m.

Figure 4. Confocal laser microscopy of HEK293(β_3)- α_v RFP cells in the presence of 45 nM LNPs at 37°C. Blue: nuclei, green: α_v RFP. Scale bar = 20 μ m. (A) The cells were treated with different LNPs and visualized after 60 min of incubation. No LNP: treated with HBSS. (B) The cells were incubated with cRGD-LNPs for 5, 10, 30 or 60 min.

Figure 5. Co-localization of cRGD-LNP with $\alpha_v\beta_3$ in HEK293(β_3)- α_v RFP cells. The cells were incubated with 45 nM LNPs for an hour at 37°C. Blue: nuclei, red: LNPs, green: α_v RFP. Scale bar = 10 μ m. (First row) The cells were incubated with cRGD-LNPs for 60 min continuously. (From the second to the fourth row) The cells were treated with LNPs and, 15 min later, the LNP solution was replaced by fresh HBSS. The incubation at 37°C was continued for another 45 min. (Bottom row) The cells were incubated with HBSS buffer only.

Figure 6. NIR *in vivo* imaging of DU145 subcutaneous tumor in mice after injections of the LNPs. NIR fluorescence images are shown for each mouse in grey levels with Min-Max values of: 0-46912. The images were taken 24 hours after injections of LNPs. L: liver, T: tumor. Graphs below the images show NIR fluorescence levels on tumors and skin. X-axis: time after injection (hours), Left Y-axis: RLU/pixel/10ms, Right Y-axis: tumor/skin ratio.

Figure 7. Fluorescence levels on the dissected organs and plasma from DU145 tumor bearing mice 24 hours after injections of the LNPs. Mean fluorescence intensities/pixel/10ms of each LNP group are shown with standard deviation.

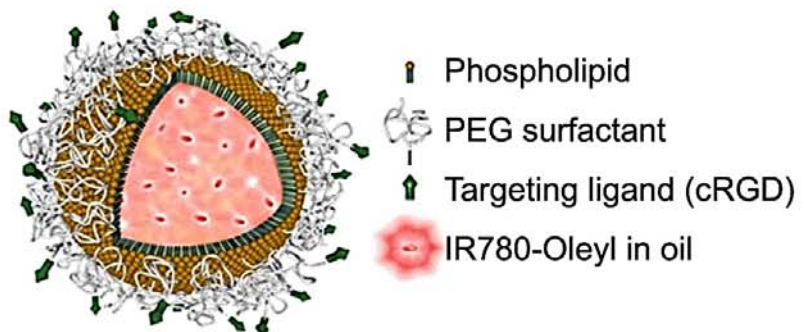
Table 1. Physico-chemical characteristics of the LNPs (triplicate values \pm SEM).

	cRGD-LNP	cRAD-LNP	LNP
Size (nm)	55 \pm 1	55 \pm 1	49 \pm 1
Polydispersity index, PDI	0.126 \pm 0.027	0.130 \pm 0.008	0.126 \pm 0.021
Zeta potential (mV)	-4.53 \pm 0.38	-4.87 \pm 0.39	-4.13 \pm 0.81

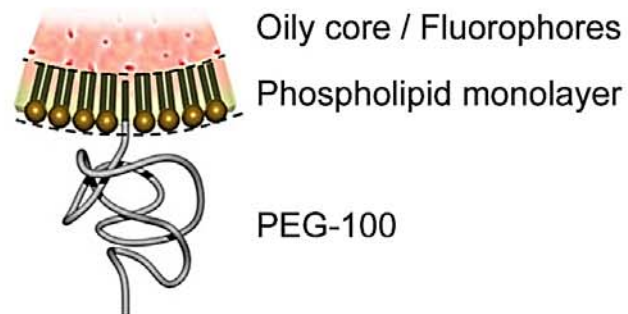
[Approximately 108 fluorophores (1.8×10^{-22} mol) per nanoparticle.]

References

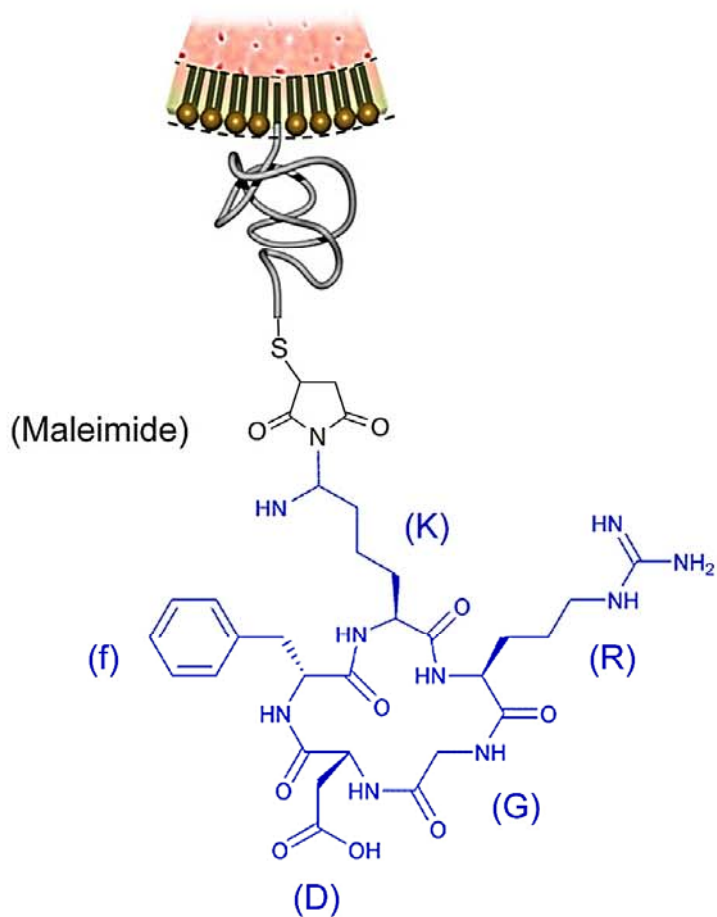
- Bridgewater, R.E., Norman, J.C., Caswell, P.T., 2012. Integrin trafficking at a glance. *J Cell Sci* 125, 3695-3701.
- Dufort, S., Sancey, L., Hurbin, A., Foillard, S., Boturyn, D., Dumy, P., Coll, J.L., 2011. Targeted delivery of a proapoptotic peptide to tumors in vivo. *Journal of Drug Targeting* 19, 582-588.
- Fang, Y., Jiang, Y., Zou, Y., Meng, F., Zhang, J., Deng, C., Sun, H., Zhong, Z., 2017. Targeted glioma chemotherapy by cyclic RGD peptide-functionalized reversibly core-crosslinked multifunctional poly(ethylene glycol)-b-poly(epsilon-caprolactone) micelles. *Acta Biomater.*
- Felding-Habermann, B., Mueller, B.M., Romerdahl, C.A., Cheresch, D.A., 1992. Involvement of integrin alpha V gene expression in human melanoma tumorigenicity. *J Clin Invest* 89, 2018-2022.
- Goutayer, M., Dufort, S., Josserand, V., Royere, A., Heinrich, E., Vinet, F., Bibette, J., Coll, J.L., Texier, I., 2010. Tumor targeting of functionalized lipid nanoparticles: assessment by in vivo fluorescence imaging. *Eur J Pharm Biopharm* 75, 137-147.
- Jacquart, A., Keramidas, M., Vollaie, J., Boisgard, R., Pottier, G., Rustique, E., Mittler, F., Navarro, F.P., Boutet, J., Coll, J.L., Texier, I., 2013. LipImage 815: novel dye-loaded lipid nanoparticles for long-term and sensitive in vivo near-infrared fluorescence imaging. *J Biomed Opt* 18, 101311.
- Karageorgis, A., Claron, M., Juge, R., Aspord, C., Thoreau, F., Leloup, C., Kucharczak, J., Plumas, J., Henry, M., Hurbin, A., Verdie, P., Martinez, J., Subra, G., Dumy, P., Boturyn, D., Aouacheria, A., Coll, J.L., 2017. Systemic Delivery of Tumor-Targeted Bax-Derived Membrane-Active Peptides for the Treatment of Melanoma Tumors in a Humanized SCID Mouse Model. *Mol Ther* 25, 534-546.
- Karageorgis, A., Dufort, S., Sancey, L., Henry, M., Hirsjarvi, S., Passirani, C., Benoit, J.P., Gravier, J., Texier, I., Montigon, O., Benmerad, M., Siroux, V., Barbier, E.L., Coll, J.L., 2016. An MRI-based classification scheme to predict passive access of 5 to 50-nm large nanoparticles to tumors. *Sci Rep* 6, 21417.
- Mas-Moruno, C., Rechenmacher, F., Kessler, H., 2010. Cilengitide: the first anti-angiogenic small molecule drug candidate design, synthesis and clinical evaluation. *Anticancer Agents Med Chem* 10, 753-768.
- Merian, J., Boisgard, R., Bayle, P.A., Bardet, M., Tavitian, B., Texier, I., 2015. Comparative biodistribution in mice of cyanine dyes loaded in lipid nanoparticles. *Eur J Pharm Biopharm* 93, 1-10.
- Sancey, L., Garanger, E., Foillard, S., Schoehn, G., Hurbin, A., Albiges-Rizo, C., Boturyn, D., Souchier, C., Grichine, A., Dumy, P., Coll, J.L., 2009. Clustering and internalization of integrin alphavbeta3 with a tetrameric RGD-synthetic peptide. *Mol Ther* 17, 837-843.
- Sutherland, M., Gordon, A., Shnyder, S.D., Patterson, L.H., Sheldrake, H.M., 2012. RGD-Binding Integrins in Prostate Cancer: Expression Patterns and Therapeutic Prospects against Bone Metastasis. *Cancers (Basel)* 4, 1106-1145.
- Xu, Y., Xu, J., Shan, W., Liu, M., Cui, Y., Li, L., Liu, C., Huang, Y., 2016. The transport mechanism of integrin alphavbeta3 receptor targeting nanoparticles in Caco-2 cells. *Int J Pharm* 500, 42-53.
- Zhong, Y., Meng, F., Deng, C., Zhong, Z., 2014. Ligand-directed active tumor-targeting polymeric nanoparticles for cancer chemotherapy. *Biomacromolecules* 15, 1955-1969.
- Zhu, Y., Zhang, J., Meng, F., Deng, C., Cheng, R., Feijen, J., Zhong, Z., 2016. cRGD-functionalized reduction-sensitive shell-sheddable biodegradable micelles mediate enhanced doxorubicin delivery to human glioma xenografts in vivo. *J Control Release* 233, 29-38.



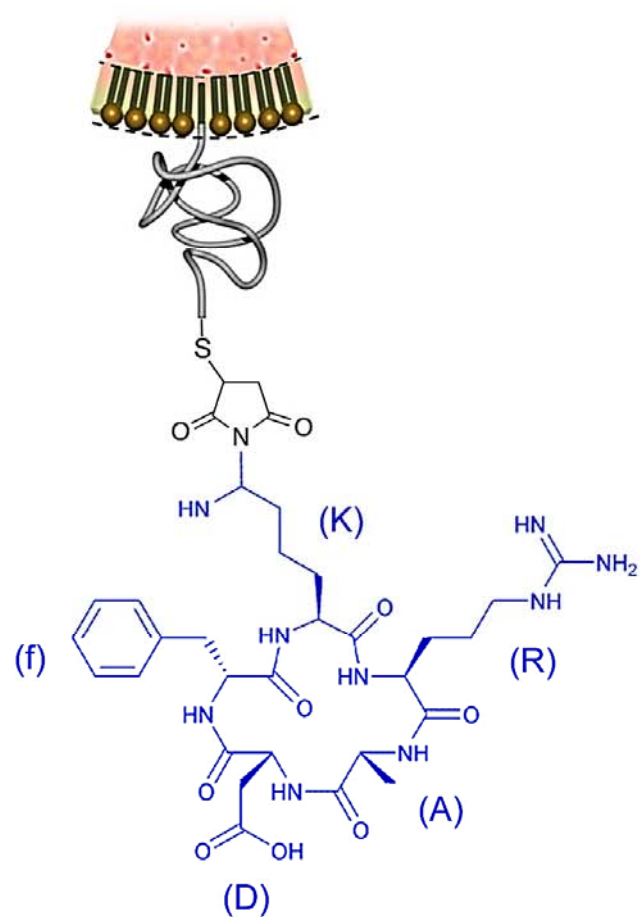
(i) Full structure



(ii) LNP

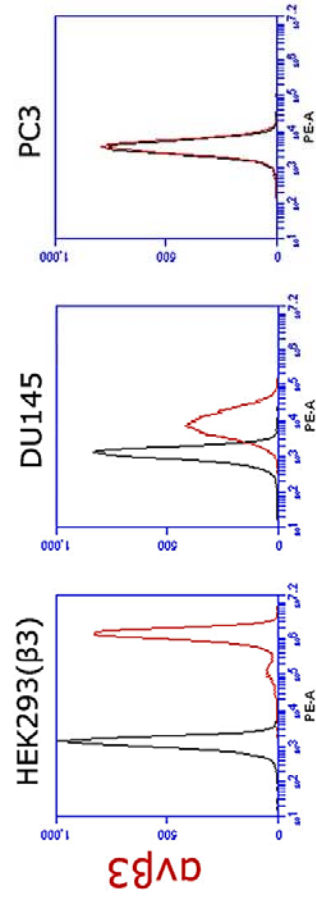


(iii) cRGD-LNP

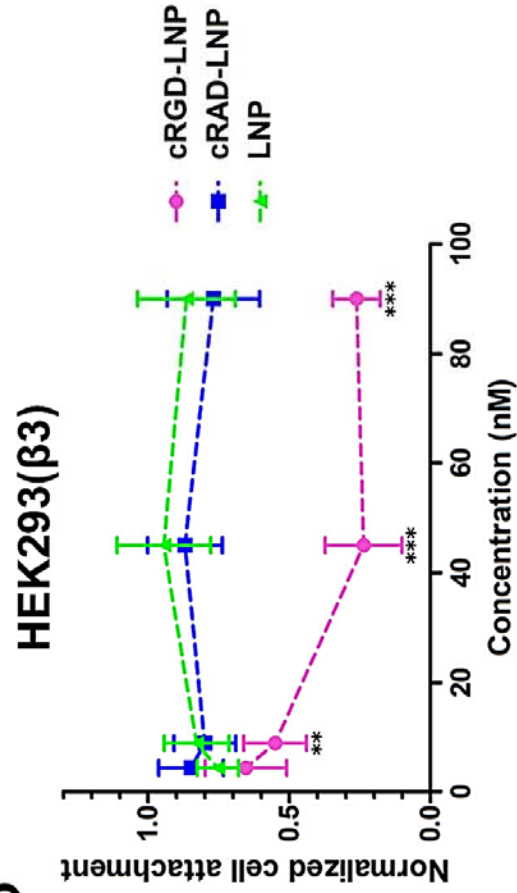


(iv) cRAD-LNP

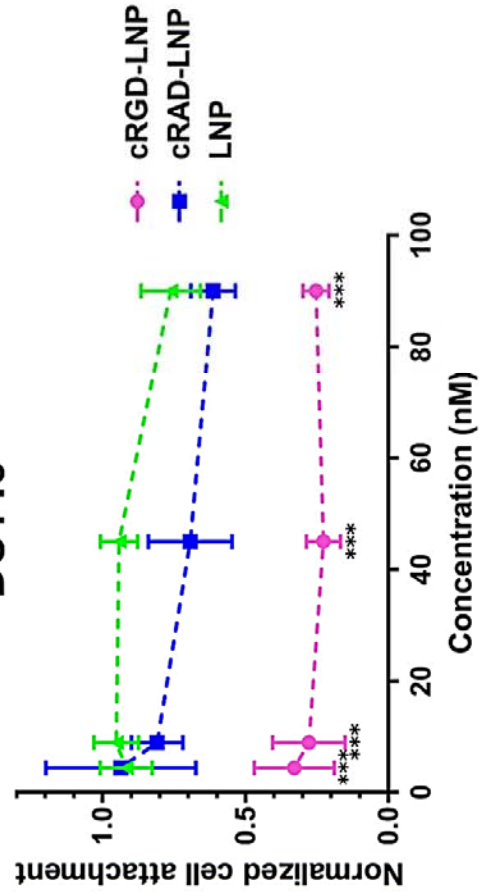
A



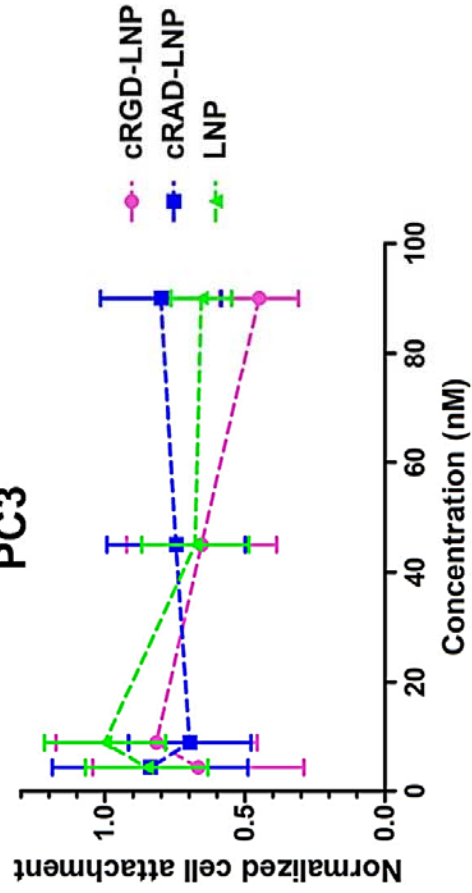
B



DU145



PC3



T0

cRGD-LNP, 45nM

cRGD-LNP, 4.5nM

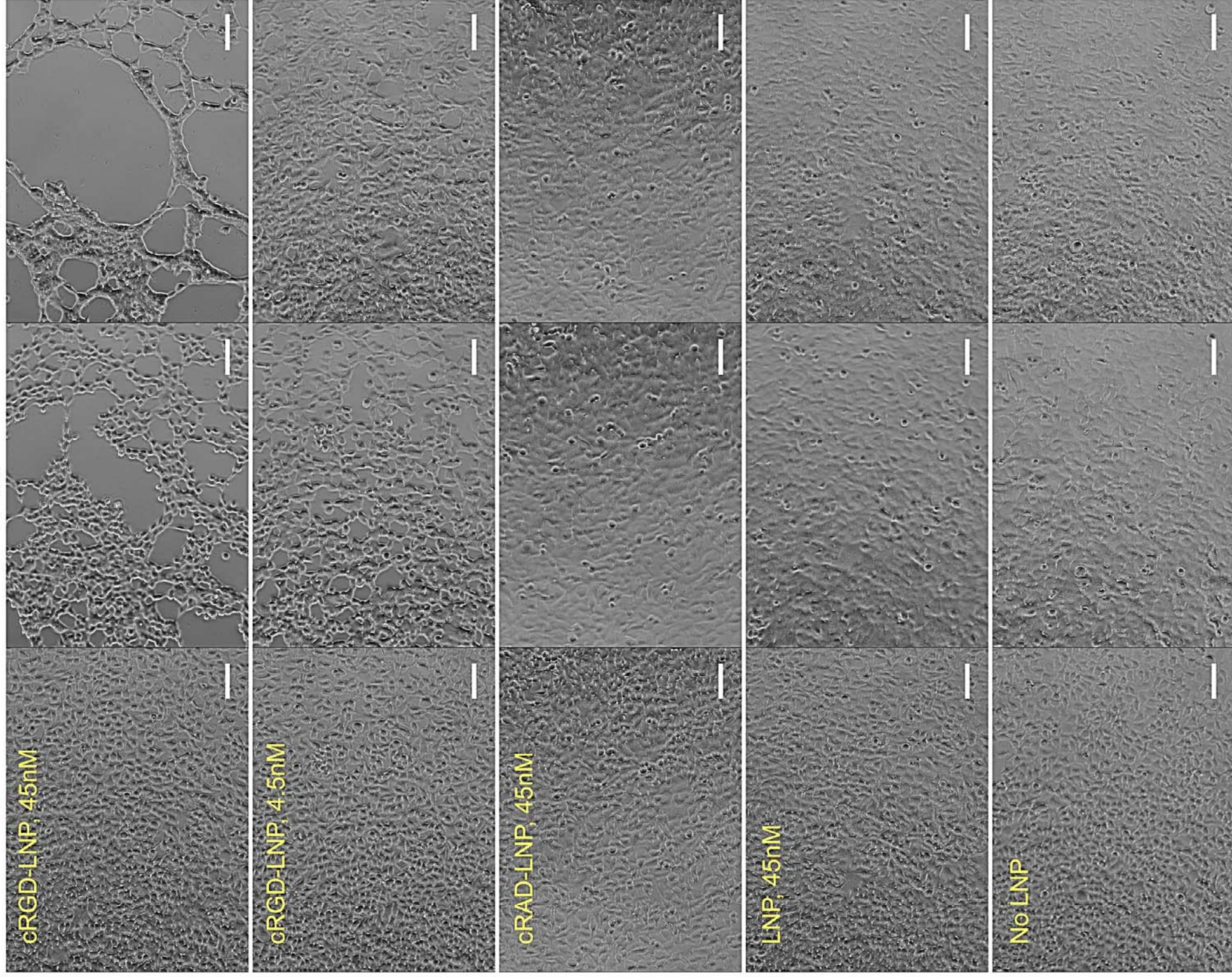
cRAD-LNP, 45nM

LNP, 45nM

No LNP

10 min

3 hr



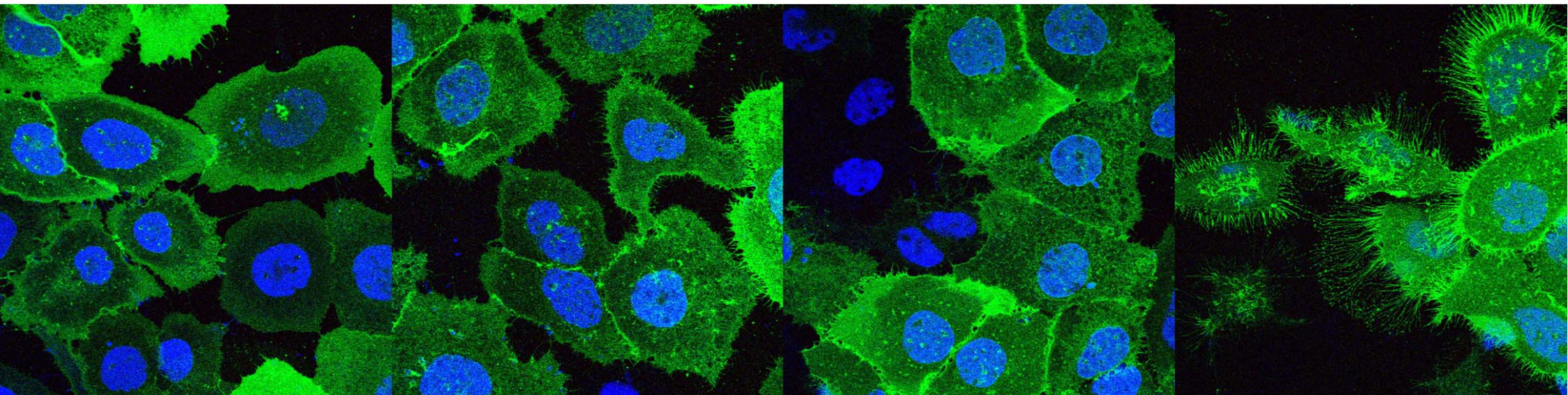
A

No LNP

LNP

cRAD-LNP

cRGD-LNP

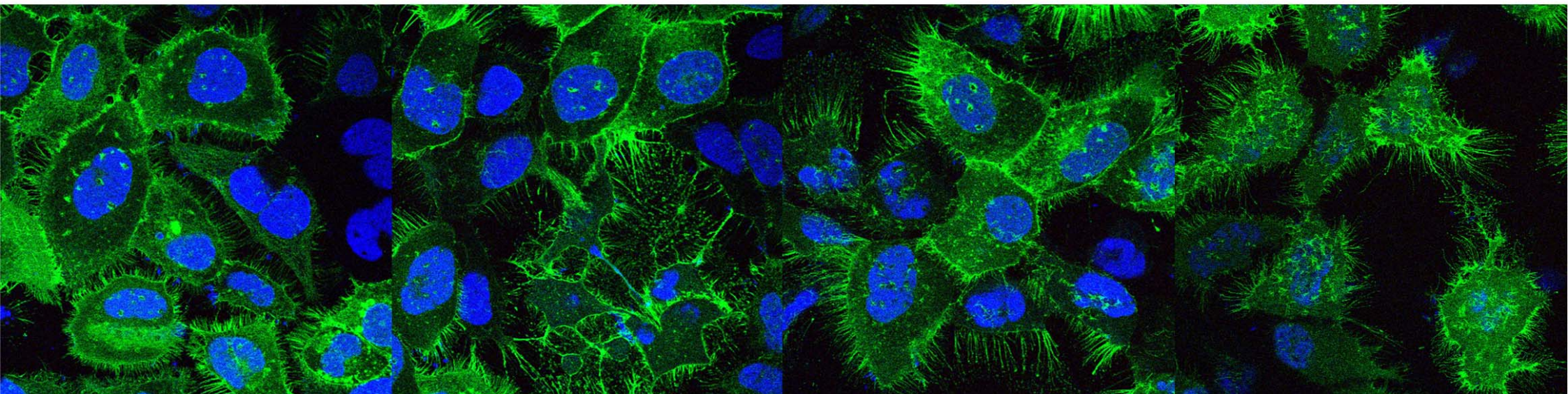
**B**

5 min

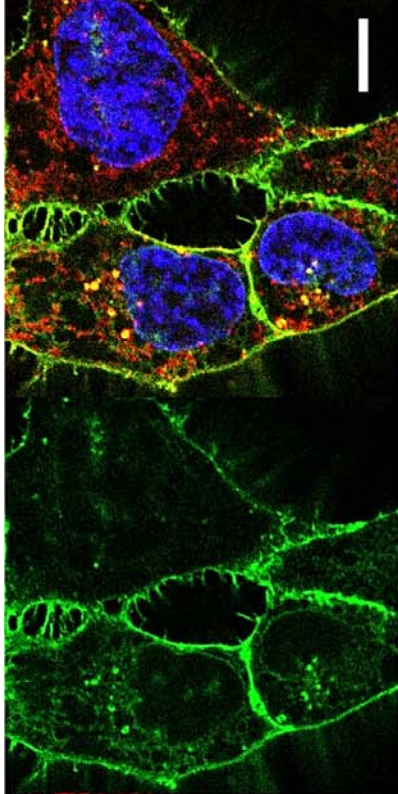
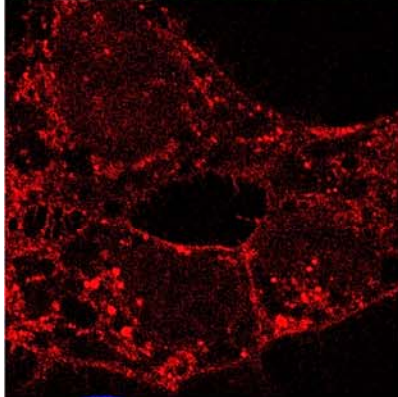
10 min

30 min

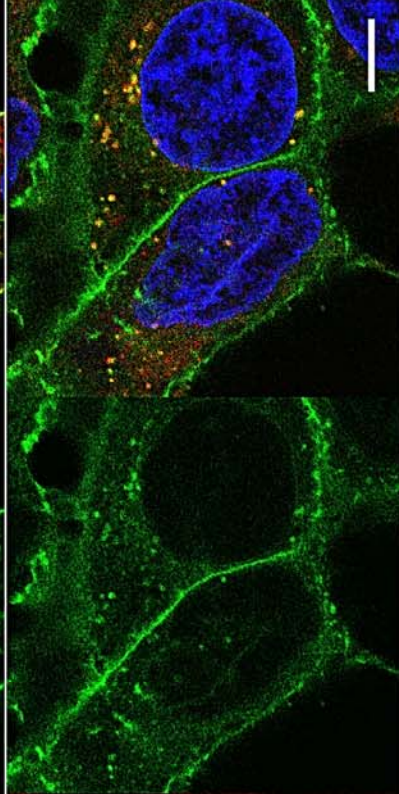
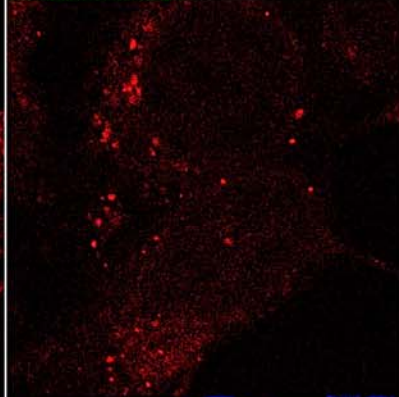
60 min



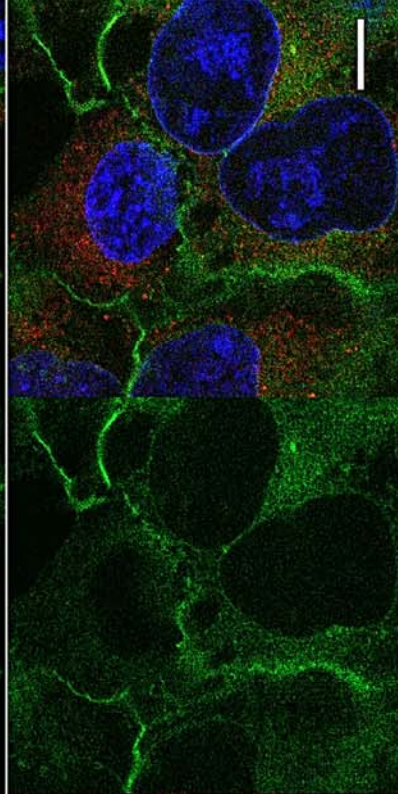
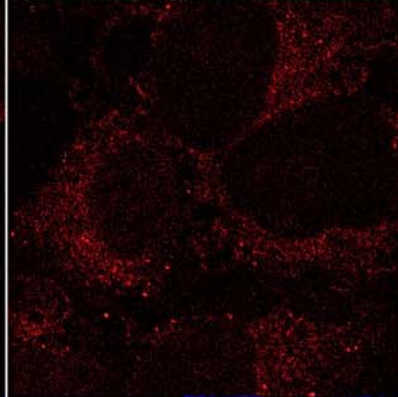
cRGD-LNP



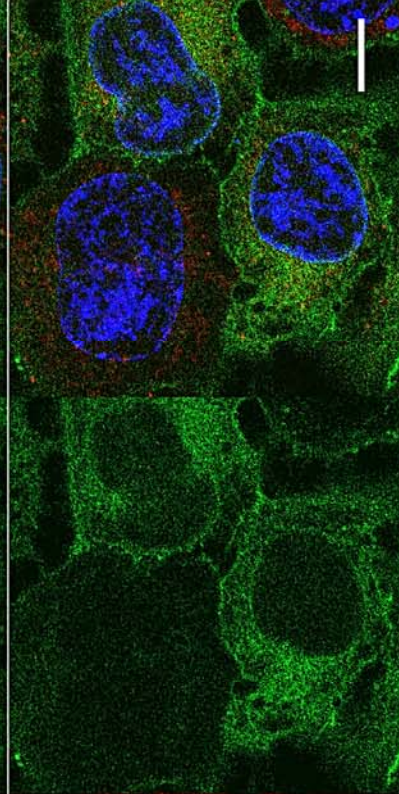
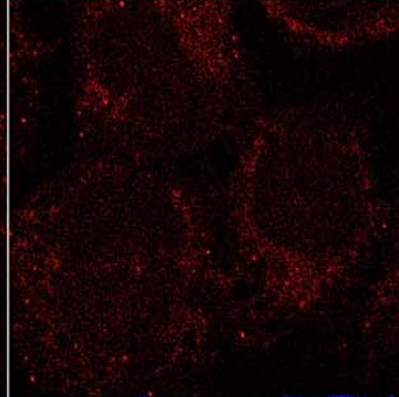
cRGD-LNP
+wash



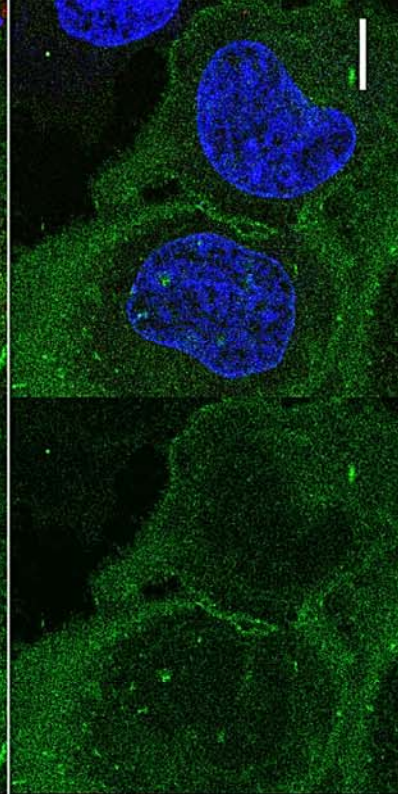
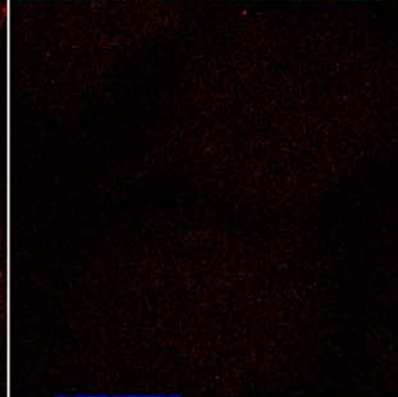
cRAD-LNP
+wash



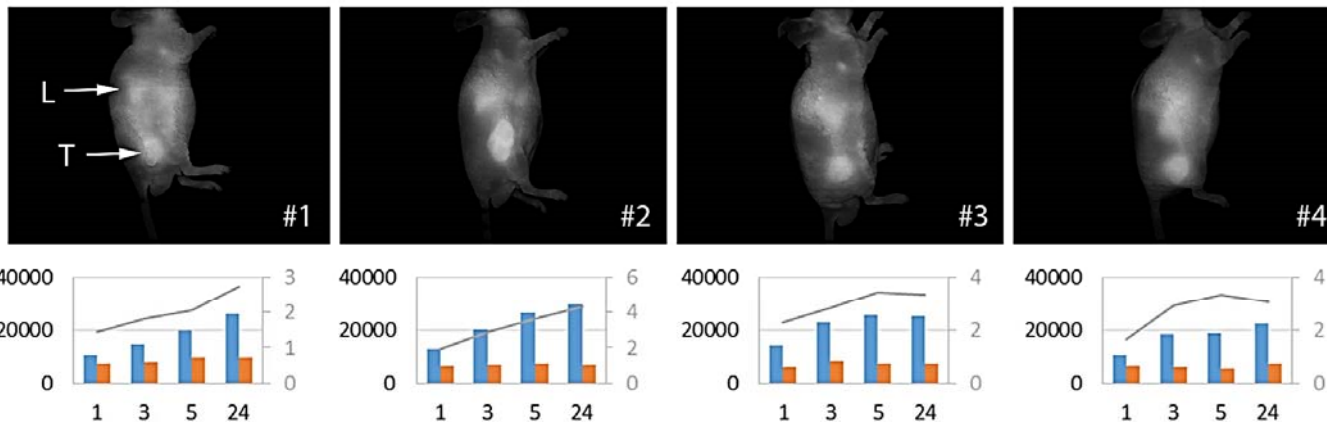
LNP
+wash



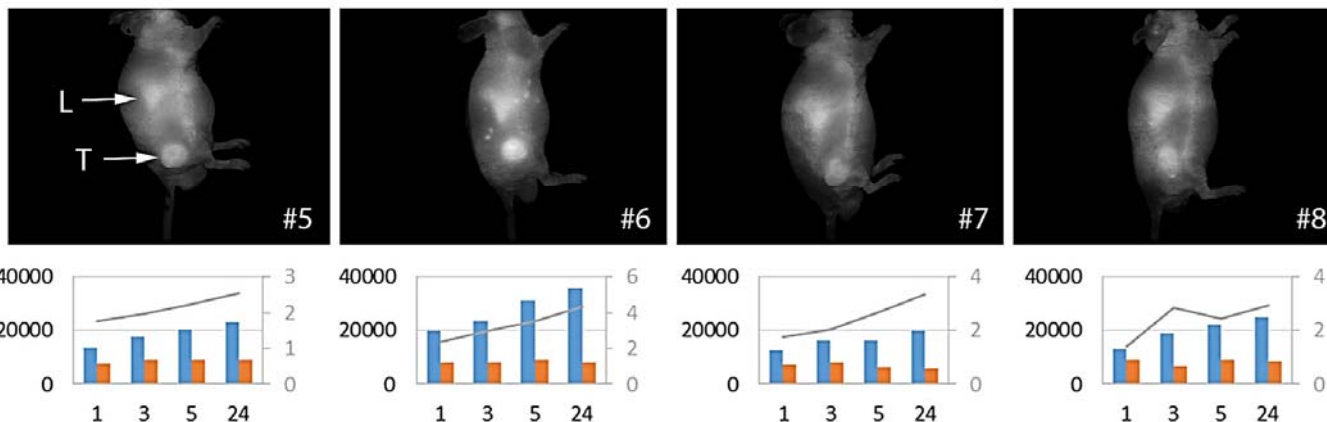
No LNP



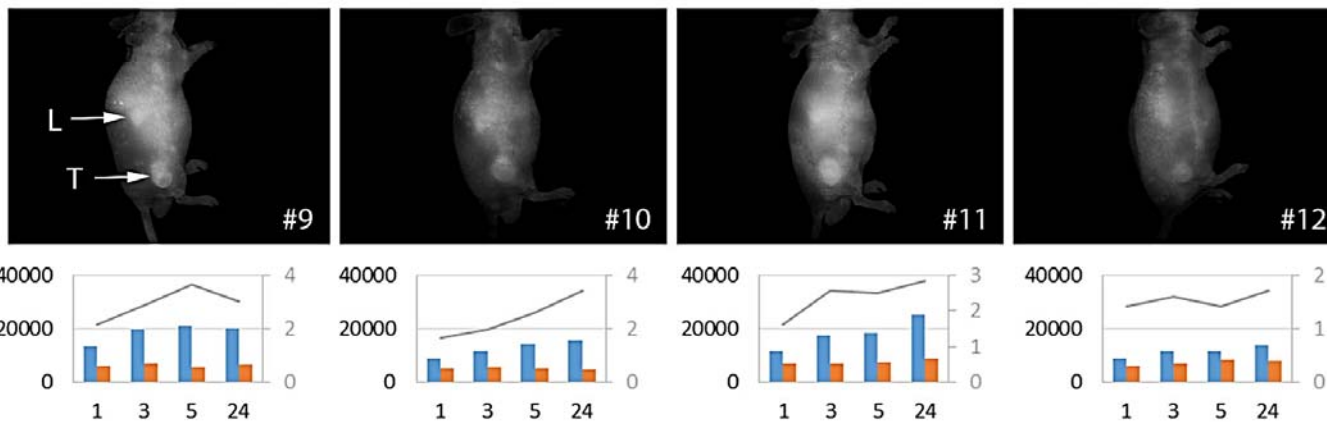
cRGD



cRAD



Std



■ tumor ■ skin — tumor/skin

